First-order normal-to-superconductor phase transition of aluminum in magnetic field by current-density functional theory for superconductors

Katsuhiko Higuchi [1] and Masahiko Higuchi[2]
[1]*Graduate School of Advanced Sciences of Matter, Hiroshima University, Higashi-Hiroshima 739-8527, Japan*
[2]*Department of Physics, Faculty of Science, Shinshu University, Matsumoto 390-8621, Japan*

(Received 29 July 2022; revised 31 October 2022; accepted 2 November 2022; published 10 November 2022)

We demonstrate that the current-density functional theory for superconductors (sc-CDFT) can describe the magnetic-field-induced first-order phase transition of aluminum from a superconducting state to a normal state. This is accomplished by introducing a model for the magnetic-field dependence of the attractive interaction between superconducting electrons. This model states that the surface potential well produced by a penetrating magnetic field leads to the magnetic-field dependence of the attractive interaction. Specifically, the electron density near the surface increases with the magnetic field owing to the surface potential well, which causes a reduction in the attractive interaction because of the screening effect. We also develop a calculation scheme to solve the gap equation of the sc-CDFT by considering the magnetic-field dependence of the attractive interaction. The calculation results for the magnetic-field dependence of the superconducting gap are in good agreement with the experimental results of the first-order phase transition.

DOI: 10.1103/PhysRevB.106.184504

I. INTRODUCTION

Density functional theory for superconductors (sc-DFT) is widely used to predict the thermal equilibrium properties of superconductors [1–31]. The sc-DFT has been extended for applications in superconductors that are immersed in a magnetic field [32–39]. The current-density functional theory for superconductors immersed in a magnetic field was developed by Kohn *et al.* [32], in which they identified the possibility of quantitatively describing the Meissner effect in conjunction with Maxwell's equations. We have recently developed the current-density functional theory for superconductors immersed in a magnetic field (sc-CDFT) [33,37–39] based on the extended constrained-search theory [40–44]. In the sc-CDFT, the electron density, transverse component of the paramagnetic current density, spin-current density, superconducting order parameter (OPSS), and its complex conjugate are chosen as the basic variables [37–41]. Thermal equilibrium values of basic variables can be reproduced using the solutions of the Bogoliubov–de Gennes–Kohn-Sham (BdG-KS) equation. Using the reproduced basic variables, we can calculate the charge density and current density. The scalar and vector potentials inside a superconductor can be obtained by substituting the obtained charge and current densities into Maxwell's equations and solving them. Substituting the obtained scalar and vector potentials into the BdG-KS equation, we obtain the charge density and current density again. The BdG-KS and Maxwell equations are solved simultaneously by continuing the above process until they become self-consistent [32,33,37–39]. Thus, it is possible not only to obtain the charge, current density, and OPSS distributions in superconductors but also to determine the scalar and vector potentials. In this way, the Meissner effect can be described by the sc-CDFT [32,33,37–39].

To solve the BdG-KS equation of the sc-CDFT, we have proposed an approximation method [37,38] in which the solutions of the BdG-KS equation are supposed to have the same spatial dependence as the single-particle wave functions of the normal state [45]. By using this approximation, the problem of solving the BdG-KS equation is reduced to the problem of finding the eigenvalues and eigenvectors of a 2×2 matrix [37,38]. Furthermore, the approximate form of the exchange-correlation energy functional of the sc-CDFT was developed by applying a mean field approximation to the attractive interaction component of the exchange-correlation energy functional [37–39]. Using the approximate form, the problem of finding the eigenvalues and eigenvectors of a 2×2 matrix is further reduced to solving the gap equation for superconductors immersed in a magnetic field [38,39]. Thus, the problem of solving the BdG-KS and Maxwell equations simultaneously is reduced to solving the gap equation of the sc-CDFT and Maxwell's equations simultaneously [38,39].

Furthermore, to perform actual calculations using the sc-DFT, we have introduced an assumption that the magnetic-field distribution obtained using the London theory [46] corresponds to that obtained by solving the BdG-KS and Maxwell equations simultaneously. Under this assumption, we have developed a calculation scheme in which the superconducting gap and attractive interaction are treated as variables that are determined by solving the gap equation of the sc-CDFT in conjunction with the energy balance equation [39]. The energy balance equation indicates that the superconducting gap in a magnetic field corresponds to the energy gain of superconducting-state electrons against normal-state electrons and is equal to the energy gain at zero magnetic field minus the potential energy of diamagnetic magnetization

[38,39]. It is found that the attractive interaction decreases as the magnetic field increases, leading to a decrease in the superconducting gap. Although the superconducting gap exhibits a first-order transition with respect to magnetic field and temperature [47,48], a previous scheme [39] could not describe the first-order phase transition experimentally observed in aluminum immersed in a magnetic field [47,48]. The reason for this discrepancy is that the attractive interaction obtained by solving the gap equation of the sc-CDFT in conjunction with the energy balance equation may be unrealistic [39].

In this paper, to describe the first-order transition observed in aluminum [47,48], we propose a model for the magnetic-field dependence of the attractive interaction and develop a calculation scheme, considering the magnetic field dependence. The present calculation scheme, which includes a mechanism for the reduction in the attractive interaction, can successfully describe the first-order transition observed in aluminum immersed in a magnetic field.

The remainder of this paper is organized as follows. In Sec. II A, an outline of the sc-CDFT is presented. In Sec. II B, we describe the magnetic field dependence of the attractive interaction in the model. The calculation scheme is presented in Sec. II C. In Sec. III, we present the calculation results and discuss how the first-order phase transition can be described using the present scheme. Finally, the conclusions are presented in Sec. IV.

II. CALCULATION SCHEME

A. sc-CDFT and its application to aluminum immersed in a magnetic field

In the sc-CDFT, the electron density, transverse component of the paramagnetic current density, spin current density, and OPSS and its complex conjugate are chosen as the basic variables [38,39]. The basic variables for the equilibrium state are calculated using the solution of the BdG-KS equation. The BdG-KS equation of the sc-CDFT is described as follows [38,39]:

$$\begin{aligned}\left(h_s^r-\mu\right)u_k(\boldsymbol{r}\zeta)+\int\{D_s(\boldsymbol{r}\zeta,\boldsymbol{r}'\zeta')-D_s(\boldsymbol{r}'\zeta',\boldsymbol{r}\zeta)\}v_k^*(\boldsymbol{r}'\zeta')d\boldsymbol{r}'d\zeta'&=E_ku_k(\boldsymbol{r}\zeta)\\ -\left(h_s^r-\mu\right)v_k(\boldsymbol{r}\zeta)+\int\{D_s(\boldsymbol{r}\zeta,\boldsymbol{r}'\zeta')-D_s(\boldsymbol{r}'\zeta',\boldsymbol{r}\zeta)\}u_k^*(\boldsymbol{r}'\zeta')d\boldsymbol{r}'d\zeta'&=E_kv_k(\boldsymbol{r}\zeta),\end{aligned}\tag{1}$$

where h_s^r denotes the single-particle Hamiltonian described as follows:

$$h_s^r=\frac{\{\boldsymbol{p}+e\boldsymbol{A}_s(\boldsymbol{r})\}^2}{2m}+v_s(\boldsymbol{r})+g\frac{\mu_B}{\hbar}\hat{\boldsymbol{s}}_{op}^{\zeta}\cdot\nabla\times\boldsymbol{A}_s(\boldsymbol{r}).\tag{2}$$

In Eqs. (1) and (2), $v_s(\boldsymbol{r})$, $\boldsymbol{A}_s(\boldsymbol{r})$, $D_s(\boldsymbol{r}\zeta,\boldsymbol{r}'\zeta')$, and $D_s^*(\boldsymbol{r}\zeta,\boldsymbol{r}'\zeta')$ are the effective potentials that are determined so that the solutions of the BdG-KS equation, $u_k(\boldsymbol{r}\zeta)$ and $v_k(\boldsymbol{r}\zeta)$, reproduce basic variables for the equilibrium state [38,39]. Specific expressions for effective potentials include the exchange-correlation energy functional of the sc-CDFT [38,39]. This functional contains both the exchange-correlation effect of the electron-electron Coulomb interaction and attractive interaction between superconducting electrons. For the exchange-correlation energy functional, we have developed an approximate form using a mean field approximation [38,39].

In this paper, the sc-CDFT is applied to an aluminum plate immersed in a magnetic field parallel to the z axis and is denoted as $(0,\ 0,\ B)$. Figure 1(a) shows a schematic of the system. The thickness of the aluminum plate is L_x and expands in the y and z directions. The dimensions of the system in the y and z directions are denoted as L_y and L_z, respectively. A periodic boundary condition is imposed on the single-particle wave functions of the normal state with periods of L_y and L_z in the y and z directions, respectively. For simplicity, a homogeneous electron gas with $r_s=2.07$ is considered, where a value of 2.07 for r_s corresponds to the density of conduction electrons in aluminum [49].

Similar to previous works [38,39], we adopt the approximation method proposed by de Gennes [45] to solve the BdG-KS equation. Namely, $u_k(\boldsymbol{r}\zeta)$ and $v_k(\boldsymbol{r}\zeta)$ are described by the multiplication of the single-particle wave functions of the normal state, $w_{k\sigma}(\boldsymbol{r})\chi_\sigma(\zeta)$, and constant coefficients; thus we obtain the following expression:

$$\begin{aligned}u_k(\boldsymbol{r}\zeta)&=\bar{u}_kw_{k\downarrow}(\boldsymbol{r})\chi_\downarrow(\zeta),\\ v_k(\boldsymbol{r}\zeta)&=\bar{v}_kw_{k\uparrow}(\boldsymbol{r})\chi_\uparrow(\zeta),\end{aligned}\tag{3}$$

where $\bar{u}_k$ and $\bar{v}_k$ denote constant coefficients, and the normal state $w_{k\sigma}(\boldsymbol{r})\chi_\sigma(\zeta)$ obeys the following equation:

$$\left(h_s^r-\mu\right)w_{k\sigma}(\boldsymbol{r})\chi_\sigma(\zeta)=\xi_{k\sigma}w_{k\sigma}(\boldsymbol{r})\chi_\sigma(\zeta).\tag{4}$$

As in previous works [38,39], we suppose that $\boldsymbol{A}_s(\boldsymbol{r})$, which should be determined by solving the BdG equation in conjunction with Maxwell's equations [32,33,37–39], is the same as the profile obtained using the London theory [46]. Particularly, $\boldsymbol{A}_s(\boldsymbol{r})$ is supposed to be given by the following expression:

$$\boldsymbol{A}_s(\boldsymbol{r})=(0,\ \lambda\bar{B}\sinh(x\lambda),\ 0)\tag{5}$$

with $\bar{B}=B/\cosh(L_x/2\lambda)$ [38,39]. Using Eq. (5) and $v_s(\boldsymbol{r})\approx 0$, h_s^r can be rewritten as follows:

$$\begin{aligned}h_s^r=\frac{p^2}{2m}+\frac{e\bar{B}\lambda}{m}\sinh\left(\frac{x}{\lambda}\right)p_y+\frac{e^2\bar{B}^2\lambda^2}{2m}\sinh^2\left(\frac{x}{\lambda}\right)\\ +\frac{e\hbar\bar{B}}{2m}\bar{\sigma}\cosh\left(\frac{x}{\lambda}\right),\end{aligned}\tag{6}$$

where $\bar{\sigma}$ is equal to 1 or -1 for a spin-up or spin-down state, respectively. Because $[h_s^r,\ p_y]=[h_s^r,\ p_z]=[p_y,\ p_z]=0$, the eigenfunction of h_s^r is described as follows [39]:

$$w_{k\sigma}(\boldsymbol{r})\chi_\sigma(\zeta)=\varphi_{k\sigma}(x)e^{i(k_yy+k_zz)}\chi_\sigma(\zeta).\tag{7}$$

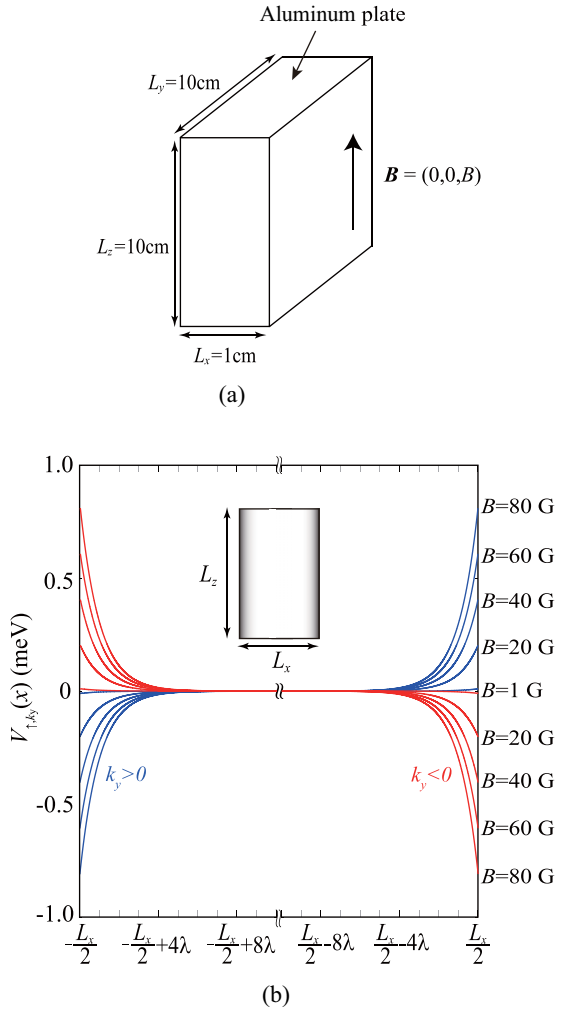

FIG. 1. (a) Schematic diagram of the system under consideration. (b) Profiles of the surface potential wells with $k_y = \pm k_F$ for several cases of B (B = 1, 20, 40, 60, 70, and 80 G). The value of λ is fixed at 50 (nm) while calculating these profiles.

Substituting Eq. (7) into Eq. (4), we obtain the following equation for $\varphi_{k\sigma}(x)$:

$$\left\{-\frac{\hbar^2}{2m}\frac{d^2}{dx^2} + V_{\sigma,k_y}(x) - \mu\right\}\varphi_{k\sigma}(x) = \left\{\xi_{k\sigma} - \frac{\hbar^2}{2m}\left(k_y^2 + k_z^2\right)\right\}\varphi_{k\sigma}(x), \tag{8}$$

where

$$V_{\sigma,k_y}(x) = \frac{e\hbar\bar{B}k_y\lambda}{m}\sinh(x/\lambda) + \frac{e\hbar\bar{B}}{2m}\bar{\sigma}\cosh(x/\lambda) + \frac{e^2\bar{B}^2\lambda^2}{2m}\sinh^2(x/\lambda). \tag{9}$$

Figure 1(b) shows a surface potential well $V_{\sigma,k_y}(x)$ formed by an effective vector potential $\boldsymbol{A}_s(\boldsymbol{r})$. The leading term of Eq. (9) is the first one that depends on k_y, B, and λ [39]. Equation (9) indicates that electrons with positive k_y tend to accumulate on the left-hand side of the plate and vice versa for electrons with negative k_y [see Fig. 1(b)], which would cause the Meissner effect [39]. It can also be observed in Fig. 1(b) and Eq. (9) that the depth of the surface potential well increases with increasing B. In other words, the electron density near the surface increases with increasing B. This implies that the attractive interaction is reduced near the surface owing to the screening effect. In the next subsection, we discuss the magnetic-field dependence of the attractive interaction caused by the surface potential well.

As mentioned in Sec. I, if the approximation method proposed by de Gennes [45] is adopted, the BdG equation can be solved by solving the gap equation of the sc-CDFT. The gap equation is as follows [37–39]:

$$1 = V_0(B)D_B(\varepsilon_F) \times \int_0^{\hbar\omega_D} \frac{\tanh\left\{\frac{\beta}{2}\left(\sqrt{\xi^2 + |\Gamma_0(B,T)|^2} - \frac{\Delta\varepsilon(B)}{2}\right)\right\}}{\sqrt{\xi^2 + |\Gamma_0(B,T)|^2}}d\xi, \tag{10}$$

where, $\Gamma_0(B,T)$, $V_0(B)$, $D_B(\varepsilon_F)$, $\Delta\varepsilon(B)$, and ω_D denote the superconducting gap, attractive interaction between superconducting electrons, density of states for normal states at the Fermi energy, average energy splitting between the up and down spin states, and Debye frequency, respectively.

We have developed a practical scheme in which the gap equation is solved in conjunction with the energy balance equation [38,39]. The energy balance equation is as follows:

$$2n^{(2)}_{\max}(B,T)\Gamma_0(B,T) = 2n^{(2)}_{\max}(0,T)\Gamma_0(0,T) - \frac{B^2}{2\mu_0}\left\{1 - \frac{2\lambda}{L_x}\tanh\left(\frac{L_x}{2\lambda}\right)\right\}\Omega, \tag{11}$$

where $2n^{(2)}_{\max}(B,T)$ and Ω denote the total number of superconducting electrons and volume of the system ($\Omega = L_xL_yL_z$), respectively. The value of $2n^{(2)}_{\max}(B,T)$ can be calculated from the OPSS and is given as follows [37–39]:

$$2n^{(2)}_{\max}(B,T) \approx \frac{D_B(\varepsilon_F)}{4}\int_0^{\hbar\omega_D}\frac{|\Gamma_0(B,T)|^2}{\xi^2 + |\Gamma_0(B,T)|^2}\tanh^2\left\{\frac{\beta}{2}\left(\sqrt{\xi^2 + |\Gamma_0(B,T)|^2} - \frac{\Delta\varepsilon(B)}{2}\right)\right\}d\xi. \tag{12}$$

Equation (11) describes the relationship between the energy gains of the superconducting state in the zero and nonzero magnetic field cases [38,39]. Equations (10) and (11) are utilized in the actual calculations, the specific procedure of which is explained in Sec. II C.

B. Model for the attractive interaction in a magnetic field

In this subsection, we describe a model for the magnetic-field dependence of attractive interaction $V_0(B)$. Assuming that the attractive interaction is approximately independent of the wave number because of the strong screening effect,

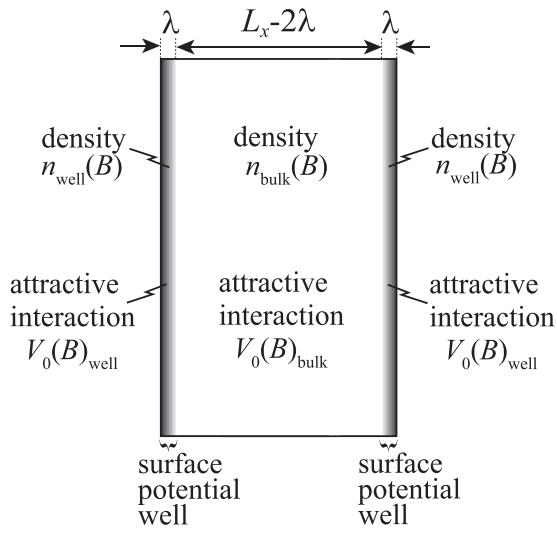

FIG. 2. Schematic diagram of the model for the magnetic-field dependence of the attractive interaction.

the magnitude of the attractive interaction at zero magnetic field, $V_0(0)$, is inversely proportional to the fourth power of the screening wave number α and volume Ω. Because the screening wave number α is given as the ratio of the plasma frequency and Fermi velocity [50], $V_0(0)$ depends on the density of the conduction electrons. Suppose that in the absence of a magnetic field the conduction electrons are uniformly distributed with the density of $n_{\rm cond}$. In this case, $V_0(0)$ is inversely proportional to $n_{\rm cond}^{3/2}$ and the volume Ω. If the proportionality constant is denoted by U, then $V_0(0)$ can be rewritten as follows:

$$V_0(0) = \frac{U}{\Omega\, n_{\rm cond}^{3/2}}, \tag{13}$$

where U is assumed to be independent of B.

In the case of $B \neq 0$, bound states are formed near the surface because of the surface potential well. The number of bound states is denoted by $2N_{\rm bound}(B)$ on both sides of the surface. A simple model is introduced to describe the magnetic-field dependence of the attractive interaction. Figure 2 shows the schematic of the model. The width of the surface potential well is approximately assumed to be λ. In addition, bound electrons are assumed to be uniformly distributed in the surface potential well. If electrons other than bound ones are distributed uniformly in the system, the total number of electrons in the surface potential well is given by $2N_{\rm bound}(B)(1-\frac{2\lambda}{L_x}) + 2\lambda L_y L_z n_{\rm cond}$. Therefore, the approximate electron density in the surface potential well is given by the following equation:

$$n_{\rm well}(B) = \left\{ n_{\rm cond} - \frac{2N_{\rm bound}(B)}{L_x L_y L_z} \right\} + \frac{N_{\rm bound}(B)}{\lambda L_y L_z}. \tag{14}$$

The density $n_{\rm well}(B)$ contributes to the screening of the attractive interaction in the region of the surface potential well. Using Eq. (13), the attractive interaction for superconducting electrons in the surface potential well region $V_0(B)_{\rm well}$ is expressed as follows:

$$V_0(B)_{\rm well} = U \frac{n_{\rm well}(B)^{-2/3}}{\lambda L_y L_z} = V_0(0) \frac{L_x}{\lambda} \left\{ \frac{n_{\rm cond}}{n_{\rm well}(B)} \right\}^{2/3}. \tag{15}$$

On the other hand, the number of electrons spread over the entire region is given by $n_{\rm cond} L_x L_y L_z - 2N_{\rm bound}(B)$. Therefore, the electron density in the bulk region is described as follows:

$$n_{\rm bulk}(B) = n_{\rm cond} - \frac{2N_{\rm bound}(B)}{L_x L_y L_z}. \tag{16}$$

Thus, the attractive interaction for superconducting electrons in the bulk region is described as follows:

$$V_0(B)_{\rm bulk} = U \frac{n_{\rm bulk}(B)^{-2/3}}{(L_x - 2\lambda) L_y L_z} = V_0(0) \frac{L_x}{L_x - 2\lambda} \left\{ \frac{n_{\rm cond}}{n_{\rm bulk}(B)} \right\}^{2/3}, \tag{17}$$

where Eq. (13) is used.

As mentioned earlier, the attraction interaction is different between the superconducting electrons near the surface and those in the bulk region. This is because the surface potential wells produce different electron densities near the surface and in the bulk, which in turn produces different screening effects. If the number of superconducting electrons in the surface potential well region is denoted by $N_s(B,T)$ on each side, the attractive interaction for $2N_s(B,T)$ superconducting electrons is described by Eq. (15), whereas for $2n_{\rm max}^{(2)}(B,T) - 2N_s(B,T)$ superconducting electrons, the attractive interaction is described by Eq. (17). Because the attractive interaction depends on the position, the following average attractive interaction is introduced as a model for the magnetic-field dependence of the attractive interaction:

$$\begin{aligned} V_0(B) &= V_0(B)_{\rm well} \frac{2N_s(B,T)}{2n_{\rm max}^{(2)}(B,T)} + V_0(B)_{\rm bulk} \left(\frac{2n_{\rm max}^{(2)}(B,T) - 2N_s(B,T)}{2n_{\rm max}^{(2)}(B,T)} \right) \\ &= V_0(0) \left[\left\{ \frac{n_{\rm cond}}{n_{\rm well}(B)} \right\}^{2/3} \frac{L_x}{\lambda} \frac{N_s(B,T)}{n_{\rm max}^{(2)}(B,T)} + \left\{ \frac{n_{\rm cond}}{n_{\rm bulk}(B)} \right\}^{2/3} \frac{L_x}{L_x - 2\lambda} \left\{ 1 - \frac{N_s(B,T)}{n_{\rm max}^{(2)}(B,T)} \right\} \right]. \end{aligned} \tag{18}$$

This model is used in solving the gap Eq. (10).

To solve the gap Eq. (10) using the attractive interaction of Eq. (18), we require the value of $N_s(B,T)$. Assuming that superconducting electrons near the surface are distributed uniformly in the width of λ, the density of the superconducting electrons $n_s(B,T)$ is described as follows:

$$n_s(B,T) = \frac{N_s(B,T)}{\lambda L_y L_z}. \tag{19}$$

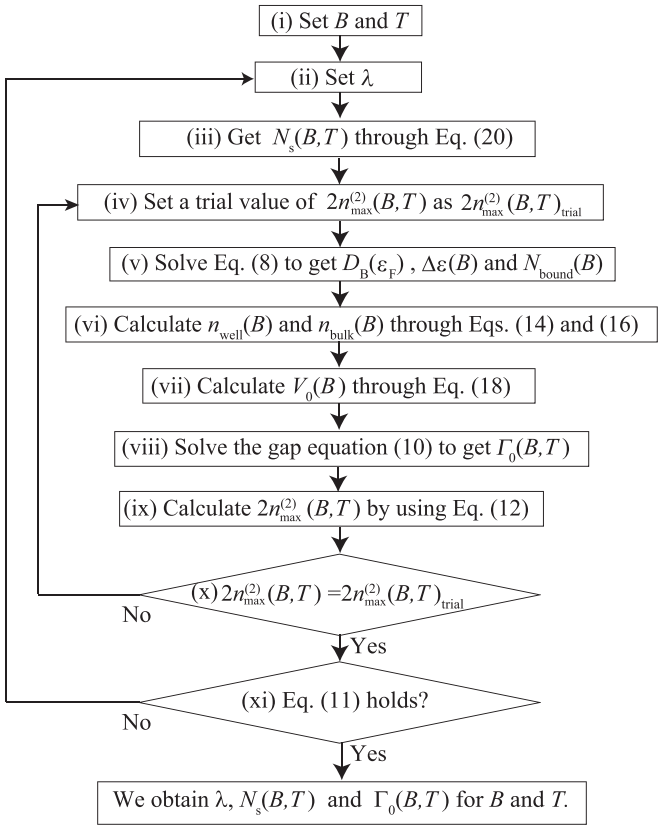

FIG. 3. Schematic of the calculation procedure.

If λ is given as the London penetration depth, then we have the following expression:

$$N_s(B,T) = \frac{mL_yL_z}{\mu_0 e^2 \lambda}. \tag{20}$$

In actual calculations, we used Eq. (20) to obtain the value of $N_s(B,T)$. The calculation procedure is discussed in the next subsection.

C. Calculation procedure

The calculation procedure is illustrated in Fig. 3. First, we set the values of B, T, and λ [steps (i) and (ii)]. In step (iii), $N_s(B,T)$ is calculated using Eq. (20). Then, in step (iv), we provide a trial value of $2n^{(2)}_{\max}(B,T)$ that appears in Eq. (18). In step (v), we solve Eq. (8) to obtain $D_B(\varepsilon_F)$, $\Delta\varepsilon(B)$, and $N_{\text{bound}}(B)$. To solve Eq. (8), we use the perturbation theory, where $V_{\sigma,k_y}(x)$ is treated as a perturbation potential. Specifically, the eigenvalues in Eq. (8) are calculated using the second-order perturbation theory. Then, in step (vi), $n_{\text{well}}(B)$ and $n_{\text{bulk}}(B)$ are calculated using Eqs. (14) and (16), respectively. In step (vii), $V_0(B)$ is calculated using Eq. (18). In steps (viii) and (ix), we obtain $\Gamma_0(B,T)$ and $2n^{(2)}_{\max}(B,T)$ by solving the gap Eq. (10). In step (x), we check whether the $2n^{(2)}_{\max}(B,T)$ obtained is consistent with the trial value provided in step (iv). Steps (iv)–(x) are repeated until consistency between the trial and the obtained values of $2n^{(2)}_{\max}(B,T)$ is achieved. After obtaining a consistent value for $2n^{(2)}_{\max}(B,T)$, we check whether Eq. (11) is satisfied by using the values of $2n^{(2)}_{\max}(B,T)$ and $\Gamma_0(B,T)$. Steps (ii)–(xi) are repeated until Eq. (11) is satisfied. Thus, we obtain the values of λ, $N_s(B,T)$, and $\Gamma_0(B,T)$ for B and T, respectively.

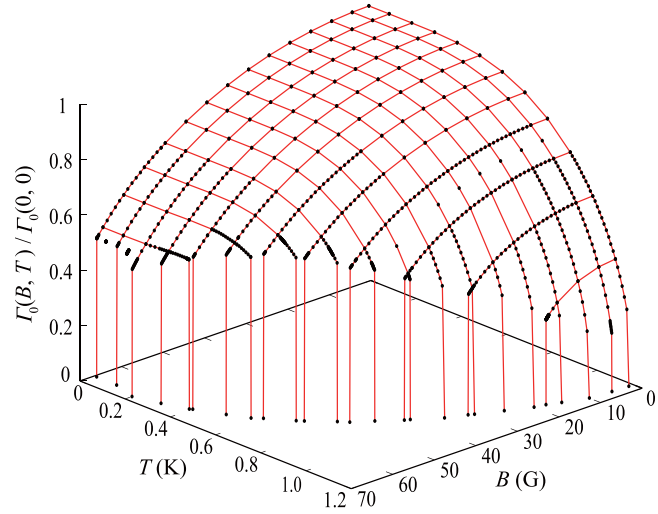

FIG. 4. Magnetic-field and temperature dependencies of the superconducting gap.

The input parameters of the present calculations are r_s and $V_0(0)$ for aluminum. Since r_s and $V_0(0)$ correspond to the density of conduction electrons and magnitude of the attractive interaction at zero magnetic field, respectively, they can be given appropriately from Refs. [38,49]. Specific values are 2.14 for r_s and 0.166 for $V_0(0)\tilde{N}(0)$, where $\tilde{N}(0)$ denotes the density of states at the Fermi energy in the case of zero magnetic field that can be calculated from r_s [38,49]. It should be noted that these parameters are independent of the magnetic field.

III. RESULTS AND DISCUSSION

Figure 4 shows the magnetic-field and temperature dependencies of the superconducting gap. The superconducting gap decreases abruptly from a finite value to zero as T or B approaches the transition temperature or the critical magnetic field. This is due to the fact that there is no solution that simultaneously satisfies Eqs. (10), (11), and (20) over the transition temperature or the critical magnetic field. This indicates that no superconducting state exists over the transition temperature or the critical magnetic field. Thus, the reproduction of the first-order phase transition observed experimentally [47,48] is reproduced using the present scheme. Figure 5 shows the magnetic-field dependence of the superconducting gap with the experimental results [48]. The calculated results well capture the characteristics of the experimental results.

A key point in describing the first-order phase transition is that the magnetic-field dependence of the attractive interaction is considered. If the mechanism of how the attractive interaction changes with a magnetic field is not considered, then the superconducting gap decreases smoothly and approaches zero with increasing T or B [39]. On the other hand, because the magnetic-field dependence of the attractive interaction is considered, the first-order phase transition is successfully reproduced, as shown in Figs. 4 and 5.

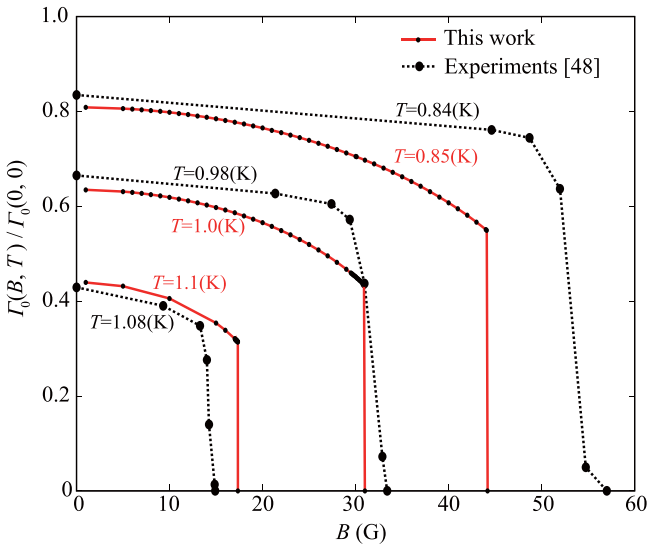

FIG. 5. Magnetic-field dependence of the superconducting gap with experimental results [49].

Next, let us discuss the magnetic-field dependence of $V_0(B)$. Figure 6 shows the magnetic-field dependence of $V_0(B)$. It is found from Fig. 6 that $V_0(B)$ gradually decreases with increasing B, which causes the decrease in $\Gamma_0(B,T)$, as shown in Figs. 4 and 5. Because $\Gamma_0(B,T)$, $N_s(B,T)$, and λ do not satisfy Eqs. (10), (11), and (20) simultaneously, as mentioned earlier, there are no calculated results for the attractive interaction in the high magnetic fields above the critical magnetic field. This is discussed later in this paper. Figure 7 shows the magnetic-field dependence of $N_s(B,T)/n^{(2)}_{\rm max}(B,T)$. This ratio represents the fraction of superconducting electrons near the surface to the total superconducting electrons. In other words, the ratio $N_s(B,T)/n^{(2)}_{\rm max}(B,T)$ indicates the fraction of superconducting electrons that are subjected to the attractive interaction weakened by the screening effect $[V_0(B)_{\rm well}]$. The ratio $N_s(B,T)/n^{(2)}_{\rm max}(B,T)$ increases with B, as shown in Fig. 7. This indicates that although the total number of superconducting electrons $2n^{(2)}_{\rm max}(B,T)$ in the sample decreases with B, as shown in Fig. 8, the superconducting electrons tend to gather near the surface. Owing to the increase in $N_s(B,T)/n^{(2)}_{\rm max}(B,T)$, $V_0(B)$ decreases with B, as shown in Fig. 6. It should be noted that the ratio $N_s(B,T)/n^{(2)}_{\rm max}(B,T)$ also represents the fraction of superconducting electrons that contribute to the antimagnetic current of the Meissner effect. It is found from Fig. 7 that the fraction of superconducting electrons contributing to the diamagnetic current increases with B.

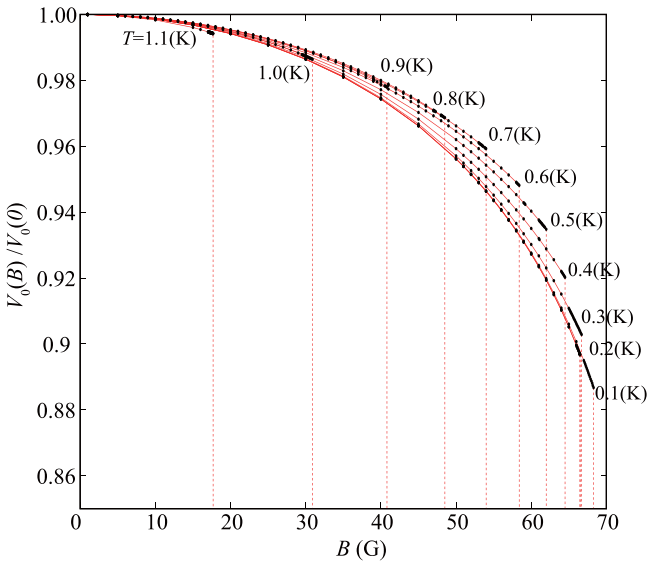

FIG. 6. Magnetic-field dependence of the attractive interaction $V_0(B)$.

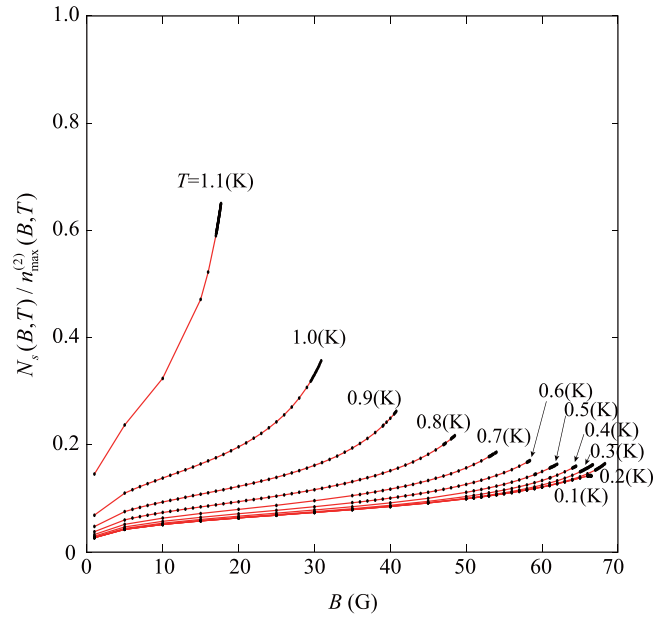

FIG. 7. Magnetic-field dependence of $N_s(B,T)/n^{(2)}_{\rm max}(B,T)$. The ratio $N_s(B,T)/n^{(2)}_{\rm max}(B,T)$ indicates the fraction of superconducting electrons that are subjected to the attractive interaction weakened by the screening effect.

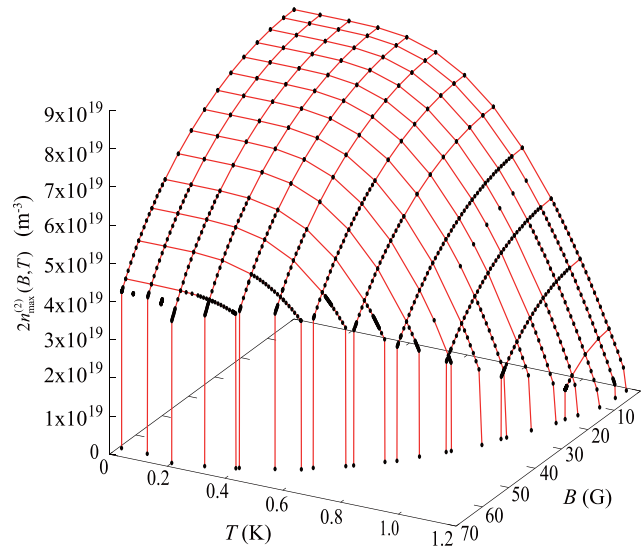

FIG. 8. Magnetic-field dependence of the total number of superconducting electrons $2n^{(2)}_{\rm max}(B,T)$.

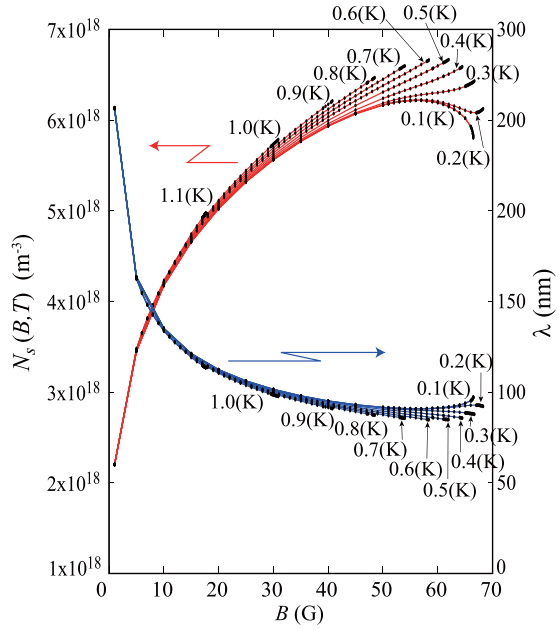

FIG. 9. Magnetic-field dependencies of λ and $N_s(B, T)$.

Figure 9 shows the magnetic-field dependence of λ and $N_s(B, T)$. In the low- and medium-magnetic-field regions, λ decreases with increasing B. Because $N_s(B, T)$ is inversely proportional to λ, as shown in Eq. (20), $N_s(B, T)$ increases with B. Therefore, the fraction of superconducting electrons that are subjected to the attractive interaction weakened by the screening effect increases with B, as shown in Fig. 7. Thus, the decrease in λ is consistent with the increase in $N_s(B, T)/n^{(2)}_{\max}(B, T)$ and decrease in $V_0(B)$. Conversely, an increase in λ leads to a decrease in $N_s(B, T)$, which may cause an increase in $V_0(B)$ because the number of superconducting electrons subjected to weak attractive interactions decreases. However, although λ increases with increasing B in the high magnetic-field region at low temperatures, as shown in Fig. 9, $V_0(B)$ decrease with increasing B, as shown in Fig. 6. This phenomenon can be explained as follows. The depth and width of the surface potential well increases with λ, leading to an increase in the electron density near the surface. Owing to the larger screening effect, $V_0(B)$ eventually decreases with B, as shown in Fig. 6. Thus, an increase in λ has opposing effects on $V_0(B)$.

If B would further increase above the critical magnetic field, λ would increase. As λ increases, the number of superconducting electrons subjected to weak attractive interactions decreases, that is, $N_s(B, T)$ decreases. This, in turn, prevents the reduction of the attractive interaction. Therefore, even if λ increases, which reduces the attractive interaction, the above-mentioned opposing effects do not cause a reduction in $V_0(B)$ at a high magnetic field above the critical magnetic field. Thus, $V_0(B)$ could not be reduced at a high magnetic field above the critical magnetic field; therefore, the solution of the simultaneous equations cannot be determined, that is, the superconducting state does not exist. Consequently, the superconducting gap disappears abruptly at the critical magnetic field, as shown in Figs. 4 and 5.

At the end of this section, we briefly comment on the physical accuracy of the calculations performed and the sensitivity of the present method to the parameters. As mentioned above, comparing the present results (Figs. 4 and 5) with the corresponding results of the previous work [39], it is found that the magnetic-field dependence of the attractive interaction, i.e., the magnetic-field dependence of the screening effect of the attractive interaction, is a key point for describing the first-order phase transition. More precisely, the number of bound states [$N_{\text{bound}}(B)$] that are formed in the surface potential well contributes sensitively to the first-order phase transition. The input parameters used in the present calculations are r_s and $V_0(0)$ for aluminum. As mentioned in Sec. II C, these parameters do not depend on the magnetic field, and are not adjusted to reach an agreement with experiments. The fact that the present calculations agree well with the experiments without the use of adjustable parameters (Fig. 5) suggests the physical accuracy and validity of performed calculations.

IV. CONCLUSION

We have developed a model for the magnetic-field dependence of the attractive interaction between superconducting electrons. The proposed model states that the surface potential well produced by a penetrating magnetic field causes a high electronic density region, which causes the magnetic-field dependence of the attractive interaction. The depth of the surface potential well increases with increasing magnetic field; thus, the attractive interaction decreases owing to the screening effect caused by the increase in the electronic density. We have also developed a calculation scheme to solve the gap equation of the sc-CDFT with considering the proposed model for the magnetic-field dependence of the attractive interaction. Specifically, the gap equation of the sc-CDFT is solved in combination with the energy balance and London penetration depth equations. It is shown that the simultaneous solution of these three equations does not exist at high magnetic fields above the critical magnetic field because of the magnetic field dependence of the attractive interaction. Thus, the first-order phase transition observed in aluminum could be reproduced using the sc-CDFT with the proposed model for the magnetic-field dependence of the attractive interaction.

ACKNOWLEDGMENT

This work was partially supported by JSPS KAKENHI Grants No. JP18K03510 and No. JP18K03461.

[1] L. N. Oliveira, E. K. U. Gross, and W. Kohn, Phys. Rev. Lett **60**, 2430 (1988).

[2] M. Lüders, M. A. L. Marques, N. N. Lathiotakis, A. Floris, G. Profeta, L. Fast, A. Continenza, S. Massidda, and E. K. U. Gross, Phys. Rev. B **72**, 024545 (2005).

[3] M. A. L. Marques, M. Lüders, N. N. Lathiotakis, Gianni Profeta, A. Floris, L. Fast, A. Continenza,

E. K. U. Gross, and S. Massidda, Phys. Rev. B **72**, 024546 (2005).
[4] T. Kreibich and E. K. U. Gross, Phys. Rev. Lett. **86**, 2984 (2001).
[5] A. Floris, G. Profeta, N. N. Lathiotakis, M. Lüders, M. A. L. Marques, C. Franchini, E. K. U. Gross, A. Continenza, and S. Massidda, Phys. Rev. Lett. **94**, 037004 (2005).
[6] G. Profeta, C. Franchini, N. N. Lathiotakis, A. Floris, A. Sanna, M. A. L. Marques, M. Lüders, S. Massidda, E. K. U. Gross, and A. Continenza, Phys. Rev. Lett. **96**, 047003 (2006).
[7] A. Sanna, C. Franchini, A. Floris, G. Profeta, N. N. Lathiotakis, M. Lüders, M. A. L. Marques, E. K. U. Gross, A. Continenza, and S. Massidda, Phys. Rev. B **73**, 144512 (2006).
[8] A. Floris, A. Sanna, S. Massidda, and E. K. U. Gross, Phys. Rev. B **75**, 054508 (2007).
[9] A. Sanna, G. Profeta, A. Floris, A. Marini, E. K. U. Gross, and S. Massidda, Phys. Rev. B **75**, 020511(R) (2007).
[10] J. Quintanilla, K. Capelle, and L. N. Oliveira, Phys. Rev. B **78**, 205426 (2008).
[11] P. Cudazzo, G. Profeta, A. Sanna, A. Floris, A. Continenza, S. Massidda, and E. K. U. Gross, Phys. Rev. B **81**, 134506 (2010).
[12] C. Bersier, A. Floris, A. Sanna, G. Profeta, A. Continenza, E. K. U. Gross, and S. Massidda, Phys. Rev. B **79**, 104503 (2009).
[13] G. Stefanucci, E. Perfetto, and M. Cini, Phys. Rev. B **81**, 115446 (2010).
[14] R. Akashi, K. Nakamura, R. Arita, and M. Imada, Phys. Rev. B **86**, 054513 (2012).
[15] R. Akashi and R. Arita, Phys. Rev. B **88**, 014514 (2013).
[16] F. Essenberger, A. Sanna, A. Linscheid, F. Tandetzky, Gianni Profeta, P. Cudazzo, and E. K. U. Gross, Phys. Rev. B **90**, 214504 (2014).
[17] G. Csire, B. Újfalussy, J. Cserti, and B. Győrffy, Phys. Rev. B **91**, 165142 (2015).
[18] F. Essenberger, A. Sanna, P. Buczek, A. Ernst, L. Sandratskii, and E. K. U. Gross, Phys. Rev. B **94**, 014503 (2016).
[19] J. A. Flores-Livas, A. Sanna, and E. K. U. Gross, Eur. Phys. J. B **89**, 63 (2016).
[20] M. Monni, F. Bernardini, A. Sanna, G. Profeta, and S. Massidda, Phys. Rev. B **95**, 064516 (2017).
[21] J. A. Flores-Livas, A. Sanna, A. P. Drozdov, L. Boeri, G. Profeta, M. Eremets, and S. Goedecker, Phys. Rev. Mater. **1**, 024802 (2017).
[22] K. Higuchi, E. Miki, and M. Higuchi, J. Phys. Soc. Jpn. **86**, 064704 (2017).
[23] A. Sanna, A. Davydov, J. K. Dewhurst, S. Sharma, and J. A. Flores-Livas, Eur. Phys. J. B **91**, 177 (2018).
[24] M. Lüders, P. Cudazzo, G. Profeta, A. Continenza, S. Massidda, A. Sanna, and E. K. U. Gross, J. Phys.: Condens. Matter **31**, 334001 (2019).
[25] G. Marini, P. Barone, A. Sanna, C. Tresca, L. Benfatto, and G. Profeta, Phys. Rev. Mater. **3**, 114803 (2019).
[26] C. Pellegrini, H. Glawe, and A. Sanna, Phys. Rev. Mater. **3**, 064804 (2019).
[27] K. Higuchi and M. Higuchi, JPS Conf. **30**, 011066 (2020).
[28] M. Kawamura, Y. Hizume, and T. Ozaki, Phys. Rev. B **101**, 134511 (2020).
[29] T. Nomoto, M. Kawamura, T. Koretsune, R. Arita, T. Machida, T. Hanaguri, M. Kriener, Y. Taguchi, and Y. Tokura, Phys. Rev. B **101**, 014505 (2020).
[30] A. Davydov, A. Sanna, C. Pellegrini, J. K. Dewhurst, S. Sharma, and E. K. U. Gross, Phys. Rev. B **102**, 214508 (2020).
[31] K. Higuchi and M. Higuchi, J. Phys. Commun. **5**, 095003 (2021).
[32] W. Kohn, E. K. U. Gross, and L. N. Oliveira, J. Phys. (Paris) **50**, 2601 (1989).
[33] K. Higuchi, K. Koide, T. Imanishi, and M. Higuchi, Int. J. Quantum Chem. **113**, 709 (2013).
[34] A. Linscheid, A. Sanna, A. Floris, and E. K. U. Gross, Phys. Rev. Lett. **115**, 097002 (2015).
[35] A. Linscheid, A. Sanna, F. Essenberger, and E. K. U. Gross, Phys. Rev. B **92**, 024505 (2015).
[36] A. Linscheid, A. Sanna, and E. K. U. Gross, Phys. Rev. B **92**, 024506 (2015).
[37] K. Higuchi, H. Niwa, and M. Higuchi, J. Phys. Soc. Jpn. **86**, 104705 (2017).
[38] K. Higuchi, N. Matsumoto, Y. Kamijo, and M. Higuchi, Phys. Rev. B **102**, 014515 (2020).
[39] K. Higuchi, N. Matsumoto, Y. Kamijo, and M. Higuchi, J. Phys.: Condens. Matter **33**, 435602 (2021).
[40] M. Higuchi and K. Higuchi, Phys. Rev. B **69**, 035113 (2004).
[41] K. Higuchi and M. Higuchi, Phys. Rev. A **79**, 022113 (2009).
[42] M. Higuchi and K. Higuchi, Phys. Rev. A **81**, 042505 (2010).
[43] K. Higuchi and M. Higuchi, Phys. Rev. B **82**, 155135 (2010).
[44] M. Higuchi and K. Higuchi, Comput. Theor. Chem. **1003**, 91 (2013).
[45] P. G. De Gennes, *Superconductivity of Metals and Alloys* (Benjamin, New York, 1966).
[46] F. London and H. London, Proc. R. Soc. A **149**, 71 (1935).
[47] D. H. Douglass Jr, Phys. Rev. Lett. **7**, 14 (1961).
[48] R. Meservey and D. H. Douglass Jr, Phys. Rev. **135**, A24 (1964).
[49] M. P. Marder, *Condensed Matter Physics* (Wiley, New York, 2000), Chap. 6.
[50] S. Raimes, *Many-Electron Theory* (North-Holland, London, 1972).